LRRK2 Suppresses Lysosome Degradative Activity in Macrophages and Microglia via Transcription Factor E3 Inhibition

Narayana Yadavalli[1,2,3,4,6], and Shawn M. Ferguson[1,2,3,4,5,6*]

Departments of Cell Biology[1] and Neuroscience[2], Program in Cellular Neuroscience, Neurodegeneration and Repair[3], Wu Tsai Institute[4], Kavli Institute for Neuroscience[5], Yale University School of Medicine, New Haven, Connecticut 06510, USA. Aligning Science Across Parkinson's (ASAP) Collaborative Research Network, Chevy Chase, MD, 20815, USA.[6]

*Correspondence: shawn.ferguson@yale.edu

Running title: LRRK2 suppresses lysosome activity

Abstract

Variants in leucine rich repeat kinase 2 (LRRK2) that increase kinase activity confer risk for sporadic and familial forms of Parkinson's disease. However, LRRK2-dependent cellular processes responsible for disease risk remain uncertain. Here we show that LRRK2 negatively regulates lysosome degradative activity in macrophages and microglia via a transcriptional mechanism. Depletion of LRRK2 and inhibition of LRRK2 kinase activity both enhance lysosomal proteolytic activity and increase the expression of multiple lysosomal hydrolases. Conversely, the kinase hyperactive LRRK2 G2019S Parkinson's disease mutant suppresses lysosomal degradative activity and gene expression. We identified transcription factor E3 (TFE3) as a mediator of LRRK2-dependent control of lysosomal gene expression. LRRK2 negatively regulates both the abundance and nuclear localization of TFE3 and LRRK2-dependent changes in lysosome protein expression require TFE3. These discoveries define a mechanism for LRRK2-dependent control of lysosomes and support a model wherein LRRK2 hyperactivity increases Parkinson's disease risk by suppressing lysosome degradative activity.

Introduction

Mutations in the *leucine rich repeat kinase 2 (LRRK2)* gene cause an autosomal dominant form of Parkinson's disease[1,2]. Additional LRRK2 variants contribute to risk for sporadic Parkinson's disease[3,4]. Human genetics studies have furthermore linked LRRK2 variants to risk for pathogen infections and inflammatory diseases[5-7]. These connections between LRRK2 and human disease raise questions about the normal functions of LRRK2 and the mechanisms whereby excessive or aberrant LRRK2 promotes disease. They have also motivated the development of LRRK2 inhibitors as a putative Parkinson's disease therapy[8].

LRRK is a large protein that contains both catalytic domains (kinase and GTPase) and scaffolding domains (armadillo, ankyrin, leucine rich repeats, C-terminal of ROC and WD40)[9]. Considerable attention has focused on the kinase activity of LRRK2 due to the fact that multiple Parkinson's disease variants increase this activity[9,10]. Although the identification of direct physiological functions of LRRK2 remains an open area of investigation, a role for LRRK2 in the endo-lysosomal pathway is supported multiple lines of evidence[9,11]. This includes the identification of specific Rab GTPases that function in the endo-lysosomal pathway as substrates for the kinase activity of LRRK2[12-14]. Furthermore, LRRK2 is recruited to the surface of damaged lysosomes where it supports repair processes[15-18]. Broader functional relevance of LRRK2 for lysosomes is supported by observations of lysosome-related phenotypes following LRRK2 inhibition or knockout in model organisms[19-23]. Interestingly, LRRK2 inhibition has been reported to enhance several aspects of lysosome function via undefined mechanisms[24-26]. In humans, LRRK2 variants that confer Parkinson's disease risk result in elevated levels of bis(monoacylglycerol) phosphate (BMP), a late endosome/lysosome enriched lipid, in the urine and cerebrospinal fluid[8]. Changes in the levels of some lysosomal hydrolases have also been reported as a consequence of such LRRK2 mutations[23,27]. While many studies have linked LRRK2 perturbations to diverse lysosome changes, there remains considerable uncertainty about underlying mechanisms. The relationship

between LRRK2 and lysosomes is part of a broader picture that has emerged that links lysosome dysfunction to Parkinson's disease pathogenesis[28,29].

Given the major impact of Parkinson's disease on midbrain dopaminergic neurons, significant attention has focused on neuronal roles for LRRK2[30-33]. However, LRRK2 is expressed in diverse non-neuronal cell types. In particular, some studies have shown that LRRK2 expression levels are notable in cells of the monocytic lineage including macrophages and microglia[5,18,34-36]. Interestingly, recent analysis of human genetics data has suggested that non-coding LRRK2 variants can confer Parkinson's disease risk via regulation of LRRK2 expression selectively in microglia[37]. Functions for LRRK2 in microglia and related myeloid cells such as macrophages are also supported by studies that have described phenotypes arising from LRRK2 perturbations in such cells[5,15,17,18,38-41]. These observations raise questions about the direct targets and pathways regulated by LRRK2 in these highly phagocytic cells.

To identify functions of LRRK2 in macrophages and microglia, we took advantage of LRRK2 mutant mouse models as well as the recent development of protocols for the differentiation of macrophages and microglia from human iPSCs to test the impact of LRRK2 genetic and pharmacological perturbations on lysosomal degradative activity in these specialized cell types. Our results from LRRK2 inhibition, LRRK2 KO and LRRK2 activating mutation (G2019S) knockin experiments revealed an inverse relationship between LRRK2 kinase activity and the proteolytic activity of lysosomes. These changes in lysosome activity arising from LRRK2 perturbations were accompanied by increases in protein and mRNA levels for multiple genes encoding lysosome proteins. In search of a mechanism to explain such broad LRRK2-dependent changes in lysosome-related gene expression, we identified a major role for LRRK2 in inhibiting the abundance and nuclear localization of transcription factor E3 (TFE3). TFE3, along with the closely related TFEB, promotes expression of genes encoding lysosome proteins by binding to response elements in their promoters[42-44]. We furthermore established a requirement for TFE3 in

promoting increased lysosome function downstream of LRRK2 inhibition. Collectively, our data supports a model wherein LRRK2 suppresses the activity of lysosomes in macrophages and microglia by negatively regulating TFE3.

Results

LRRK2 suppresses lysosome degradative activity in human and mouse macrophages

To investigate the relationship between LRRK2 and lysosome degradative activity, we took advantage of an established protocol to differentiate control and LRRK2 KO human iPSCs into macrophages[45]. Tubular lysosomes were robustly labeled in these macrophages following incubation with Alexa488-BSA and DQ-BSA (a reporter of lysosome protease activity that is taken up by endocytosis and concentrated within lysosomes[46], Fig. 1A). This combination of probes allows the measurement of lysosomal proteolytic activity while controlling for potential changes in endocytic uptake. Inhibition of LRRK2 kinase activity in control macrophages with either Mli-2 or LRRK2-in-1 resulted in an increase in the DQ-BSA signal without affecting the Alexa488-BSA signal (Fig. 1B and C). A similar selective increase in the DQ-BSA signal was observed in LRRK2 KO macrophages and this was not further enhanced by either of the LRRK2 inhibitors (Fig. 1B and C). The lack of any additional effect of these inhibitors on the LRRK2 KO cells argues against any major off target effects of these drugs on lysosomal proteolytic activity in these experiments.

To test the generalizability of these results, we performed additional experiments in both wildtype and LRRK2 KO mouse bone marrow derived macrophages (BMDMs). In each case, the KO of LRRK2 or inhibition of its kinase activity resulted in an increase in lysosomal protease activity as measured by the DQ-BSA assay (Fig. S1 A and B).

LRRK2 G2019S Parkinson's disease mutant suppresses macrophage lysosome proteolytic activity

Based on the increased lysosome proteolytic activity following genetic and pharmacological inhibition of LRRK2, we predicted that the gain-of-function LRRK2 G2019S Parkinson's disease mutant which has increased kinase activity would have the opposite effect. Indeed, macrophages derived from human iPSCs with a knockin of the G2019S mutation had reduced lysosomal protease activity and this was rescued by LRRK2 inhibition (Fig. 1D and E). The same was true in BMDMs from G2019S knockin mice (Fig. S1C and D).

LRRK2 negatively regulates the abundance of multiple lysosomal proteins

We next performed immunoblotting experiments on human iPSC-derived macrophages to determine whether the LRRK2-dependent changes in lysosome proteolytic activity arose from changes in the overall abundance of lysosome proteases. The experiments revealed increases in the levels of cathepsins B, C, D and L in response to either LRRK2 KO or incubation with LRRK2 inhibitors and the effects of the KO and the inhibitors were not additive (Fig. 2A-E). These effects were not limited to lysosomal proteases as levels of glucosylcerebrosidase (GCase), a Parkinson's linked lysosomal enzyme involved in glycosphingolipid metabolism, also increased in response to LRRK2 inhibition (Fig. 2A and F)[47]. This effect also extended to LAMP1, a major membrane glycoprotein of lysosomes (Fig. 2A and G). Similar changes were observed in WT versus *LRRK2* KO mouse bone marrow derived macrophages (Fig. S2A-D). Meanwhile, knockin of the *LRRK2* G2019S mutation in both human iPSC-derived macrophages and mouse bone marrow derived macrophages resulted in reduced levels of lysosome hydrolases and LAMP1 and this was reversed by LRRK2 inhibition (Fig. 3A-G and S3A-D).

LRRK2 suppresses the abundance of mRNAs encoding multiple lysosome proteins

Cathepsins are delivered to lysosomes in "pro" forms and then undergo activation via proteolytic processing upon their delivery to the lysosome lumen. As a result, they exhibit band patterns on immunoblots that reflect this coupling between trafficking and processing. LRRK2 genetic and

pharmacological perturbations increased all forms of these cathepsins and not just the abundance of their mature forms (Figure 3 and S3). As this argued for an increase in cathepsin synthesis, we next performed qRT-PCR and observed that LRRK2 KO and LRRK2 inhibition both resulted in an increase in the abundance of multiple transcripts that encode lysosomal hydrolases (Fig. 4A-D). Meanwhile, these transcripts were down-regulated in G2019S knockin macrophages and this was rescued by LRRK2 inhibition (Fig. 4E-H).

LRRK2 negatively regulates TFE3

In search of an explanation for how LRRK2 regulates the expression of multiple genes that encode lysosome proteins, we next focused on the TFE-MITF family of transcription factors (TFEB, TFE3, TFEC and MITF) as they coordinate the expression of gene encoding lysosome proteins by binding to a response element (CLEAR motif) that is found in their promoters[43,48-50]. Past studies have shown that these transcription factors are highly regulated at the level of their nuclear versus cytoplasmic distribution[42,50-52]. TFE3 stands out for having high expression macrophages and in microglia within the mouse brain[53]. We therefore took advantage of an anti-TFE3 antibody that robustly detects the endogenous protein in immunofluorescence assays to test the effect of LRRK2 perturbations on TFE3 subcellular distribution. While TFE3 was mostly excluded from the nucleus of control iPSC-derived macrophages (Fig. 5A and B), it became concentrated in the nucleus following LRRK2 inhibition (Fig. 5A and B). Furthermore, TFE3 was constitutively enriched in the nucleus in LRRK2 KO cells (Fig. 5A and B). This LRRK2-dependent negative regulation of TFE3 nuclear localization was also observed in mouse BMDMs in response to LRRK2 inhibition and KO (Fig. S4A and B). Meanwhile, both human and mouse macrophages with a knockin of the LRRK2 G2019S mutation had weak cytoplasmic TFE3 immunofluorescence and this became brighter and was concentrated in the nucleus in response to LRRK2 kinase activity inhibition (Fig. 5C and D; S4C and S4D). In support of a causal role for TFE3 in the LRRK2-

dependent changes in lysosomal gene expression, following siRNA-mediated knockdown of TFE3, LRRK2 inhibition no longer resulted in an increase in lysosome proteins (Fig. 5E).

Interestingly, in addition to translocating to the nucleus, TFE3 protein levels increased in response to LRRK2 inhibition with MLi-2 and this was suppressed by treatment with TFE3 siRNA (Fig. 5E). This effect of MLi-2 was on target as it was also seen following treatment LRRK2-In-1 and in response to LRRK2 KO in human and mouse macrophages (Fig. 6A and B; S4E and F). Meanwhile, TFE3 protein levels were lower in LRRK2 G2019S human and mouse macrophages and this was rescued by treatment with MLi-2 (Fig. 6C and D; S4G and H). qRT-PCR assays revealed reciprocal effects of LRRK2 inhibition and the G2019S mutation on TFE3 transcript abundance (Fig. 6E). These results suggest that TFE3 may positively regulate its own expression via a positive feedback loop.

LRRK2-dependent regulation of microglial lysosomes

Given the impact of LRRK2 mutations in Parkinson's disease, the close functional relationship between macrophages and microglia and recent genetic insights into the potential importance of microglial LRRK2 in Parkinson's disease, we next differentiated human iPSCs into microglia via an established protocol[37,54]. Similar to what was described above for macrophages, LRRK2 negatively regulated human microglial lysosome proteolytic activity (Fig. 7A-B), abundance of lysosome proteins (Fig. 7C-H) and TFE3 protein levels (Fig. 7I-J).

Discussion

Our results demonstrate that the degradative activity of lysosomes in macrophages and microglia are negatively regulated by LRRK2. We furthermore identified changes in the expression of multiple lysosomal proteins in response to LRRK2 perturbations and identified TFE3 as a mediator of the effects of LRRK2 on lysosome gene expression. These results reveal a new transcriptional mechanism for LRRK2-dependent regulation of lysosomes and suggest that

excessive suppression of lysosome activity by LRRK2 mutations may contribute to Parkinson's disease risk.

A role for LRRK2 in suppressing lysosomal activity in macrophages and microglia is seemingly at odds with the major role played by lysosomes in degrading heavy loads of cargoes that are ingested by high rates of phagocytosis that are central to the scavenger and innate immunity functions of these specialized cells. However, building on the recently proposed roles for LRRK2 in the repair of damaged lysosomes[15,16], we speculate that LRRK2-dependent inhibition of TFE3 may provide a mechanism to protect cells from excessive lysosome activity by acting as a brake on the expression of genes encoding lysosome proteins when lysosome integrity is impaired. Such a brake, might be particularly relevant in macrophages and microglia as these cells require maximally degradative lysosomes to meet the demands imposed by their highly phagocytic nature but this also makes them vulnerable to perturbations to lysosome integrity[15,16,55]. Thus, when macrophage/microglia lysosome membranes are damaged, LRRK2 can act in parallel to both support local lysosome membrane repair processes and to suppress MiT-TFE transcription factors in order to limit the potential for leakage of lysosomal hydrolases into the cytoplasm and the initiation of cell death processes that occur downstream lysosome membrane permeablization[55].

The existence of dominantly inherited LRRK2 variants that increase LRRK2 kinase activity and confer Parkinson's disease risk has stimulated the development and clinical testing of inhibitors of LRRK2 kinase activity as a potential Parkinson's disease therapy[8]. While the mechanisms linking LRRK2 dysfunction to Parkinson's disease pathogenesis may involve aberrant phosphorylation of multiple LRRK2 substrates across a range of cell types, a link to late endosomes/lysosomes is supported by observations from animal models and humans[8,20]. Bis(monoacylglyceryl)phosphate (BMP), a lipid that is enriched in the membranes of intraluminal vesicles of late endosomes and lysosomes and that is secreted by the fusion of these organelles

with the plasma membrane is a biomarker of human Parkinson's disease-linked LRRK2 mutations and associated with the development of Parkinson's disease in LRRK2 mutation carriers[56]. Recent clinical trials in humans have established the in vivo efficacy of LRRK2 inhibition in lowering LRRK2 activity and normalizing urinary levels of BMP[8,22].

The ability of TFE3 (and the closely related TFEB and MITF) to promote the expression of multiple genes that encode lysosomal proteins by binding to a distinct response element in their promoters has generated considerable interest in the development of strategies to enhance their activity as a strategy to boost lysosome function across multiple disease states[57-60]. Our discovery that LRRK2 inhibition promotes nuclear localization of TFE3 and the expression of genes encoding lysosome proteins in macrophages and microglia suggests that LRRK2 inhibitors under development for Parkinson's disease might have wider impacts in the treatment of other diseases associated with lysosome deficiencies. However, while enhancing the degradative activity of lysosomes may be attractive across a range of disease states, it remains to be determined whether the lysosome abnormalities such as those observed in animal models following genetic and pharmacological inhibition of LRRK2 will limit the feasibility of long term LRRK2 inhibition in humans[22,61]. Ongoing clinical trials will soon begin to answer these questions[8].

It remains to be determined how LRRK2 fits into the complex network of regulatory machinery upstream of the MiT-TFE transcription factors. The nuclear versus cytoplasmic distribution of these proteins is tightly regulated by phosphorylation[42]. Although this has not yet been established, LRRK2 could potentially directly phosphorylate TFE3. Rag GTPases recruit TFE3 to the surface of lysosomes and bring it into proximity with mTORC1 which in turn phosphorylates MiT-TFE proteins on multiple sites that promote their cytoplasmic retention[42,51,52,62]. Therefore, novel targets for LRRK2 in the machinery that recruits MiT-TFE proteins to lysosomes also represent candidates for linking LRRK2 kinase activity to MiT-TFE regulation. Additionally, phosphorylation of Rab GTPases by LRRK2 could change the composition of lysosomes by

regulating intracellular membrane traffic and thus affect TFE3 lysosome recruitment and phosphorylation[14]. Recently described membrane remodelling properties of LRRK2 might also play a role[63]. Alternatively, defects in lysosome membrane integrity following LRRK2 depletion or inhibition could result in the release of lysosomal calcium and calcineurin-mediated dephosphorylation of TFE3 proteins[15,64-66]. Determining how LRRK2 communicates with TFE3 will require a careful dissection of these candidate pathways.

In summary, we have identified a new role for LRRK2 in the transcriptional regulation of lysosomal degradative activity in macrophages and microglia. While our research has focused on the relationship between LRRK2 and lysosomes in macrophages and microglia, LRRK2-dependent inhibition of TFE3 may also explain previously reported effects of LRRK2 mutations and inhibition on the levels of various lysosome proteins in astrocytes and neurons[23,24]. Having defined a mechanism for LRRK2-dependent suppression of the degradative activity of lysosomes, it will next be important to determine the contributions of such regulation to both normal cell biology and to Parkinson's disease risk. Our results furthermore suggest new opportunities for exploring the use of LRRK2 inhibitors to enhance lysosome activity in other diseases associated with lysosome dysfunction.

Methods

Antibodies and chemicals. The following antibodies were used in this study: GAPDH (EnCor biotechnology Inc, # MCA-1D4), human specific cathepsin D (R&D systems #AF1014), mouse specific cathepsin D- (R&D systems #AF1061), human cathepsin B (R&D systems #AF953), human cathepsin L (R&D systems # AF952), mouse cathepsin L (R&D systems # AF1515), human cathepsin C (R&D systems #AF1071), human GBA (R&D systems #MAB7410), hLAMP1 (Cell signaling Technology # 9091), mouse LAMP1 (DSHB #ID4B), MITF (Cell signaling

Technology # 125903), human TFEB (Cell signaling Technology #37785), mouse TFEB (Proteintech #13372-1-AP), TFE3 (Sigma #HPA023881). The following chemicals were used: Y-27632 Rock inhibitor (Tocris Bioscience), Mli2 (Abcam #254528), LRRK2-IN-1 (Tocris Bioscience # 4273), EDTA (Invitrogen#15575-038).

iPSC culture. Human female iPSCs (A18945) were purchased from Gibco. A18945 iPSCs with LRRK2 KO and G2019S mutations were kindly provided by Mark Cookson (NIH)[67]. These cells were cultured on Matrigel (Corning)-coated dishes in E8 media (Life Technologies) and passaged every 3rd day using 0.5mM EDTA in phosphate buffered saline.

Differentiation of iPSCs into Macrophages and Microglia. For microglia or macrophage differentiation, iPSCs were first differentiated to hematopoietic progenitor cells (HPSCs) using the STEMdiff kit (STEMCELL Technologies #5310) as per the manufacturer's instructions. These cells were further differentiated into macrophages by culturing in media containing RPMI (Gibco #11875-135), 20% FBS (Gibco) and 100ng/ml MCSF (Peprotech#300-25) as described previously for 7 days[45]. HPSCs were also differentiated to microglia via an established protocol[54]. Briefly, 100,000 HPSCs were plated on Matrigel-coated plates on day 0 in media containing DMEMF/12 (Gibco #11330-032), 2X Insulin-Transferrin-Selenite (Gibco #41400045), 5mg/ml Insulin, 1X non-essential amino acids (Gibco #11140050), 1X Glutamax (Gibco #35050061), 2X B27 (Gibco #17504-044), 0.5X N2 (Gibco #17502-048), 400uM monothiol glycerol, 100ng/ml IL34 (Peprotech # 200-34), 50ng/ml TGFbeta (Peprotech100-21), 25ng/ml MCSF (Peprotech # 300-25). Then 1 ml media was added every alternative day for next 24 days. On day 25, media was switched to 2 additional cytokines: 100ng/ml CXCL3 (Peprotech #300-31), 100ng/ml CD200 (Novoprotein #C311). On day 27 cells were fed with the 5-cytokine media and on day 28 cells were processed for the respective experiments.

Bone Marrow Derived Macrophage (BMDM) differentiation and maintenance. For mouse bone marrow-derived macrophage (BMDMs) primary cultures, each experiment involved age

and sex matched C57BL/6 mice between 3-6 months of age. *Lrrk2* KO (Lrrk2$^{tm1.1Mjff}$) and G2019S (*Lrrk2*$^{tm1.1Hlme}$) homozygous knockin mice were obtained from The Jackson Laboratory[68]. Mice were euthanized via CO_2 or isoflurane inhalation and cervical dislocation. Femurs were collected and cavities were flushed with 5ml ice-cold PBS and the bone marrow cells were collected by centrifugation. The resulting pellet was resuspended and differentiated for 6 days in culture media containing: DMEMF12 (Gibco, #11330-032) supplemented with 20% FBS (Gibco, #16140-071), 20% L929 conditioned media, 1% penicillin-streptomycin (Gibco, # 15140-122) and 1%GlutaMAX^{TM} (Gibco, # 35050061).

Microscopy. All microscopy experiments were performed on a Zeiss 880 Airyscan confocal microscope using a 63X plan-apochromat objective (1.46 NA). Images were acquired with Zeiss Zen Black software. Further analysis was performed by using FIJI/ImageJ[69].

DQ-BSA assay. 100,000 macrophages or microglia were seeded on Mattek glass bottom dishes. The next day cells were treated with 50 nM MLi2 or 250 nM LRRK2-IN-1 for 2 hours followed by 1 hour treatment with 10ug/ml DQ-BSA (Thermo Fisher Scientific, #D12051) and 50ug/ml Alexa-488 BSA (Thermo Fisher Scientific #A13100) in the media containing inhibitors. After 3 hours the cells were washed 3X with media and imaged. For DQ-BSA quantification, maximal projection images from z-stacks spanning complete cells were segmented in FIJI/ImageJ using the find maxima function. Then duplicated images were threshold by default algorithm. The segmented and thresholder images were next combined by AND function to create a mask. Finally, mean gray values were obtained by applying analyze particle function to the mask and redirecting this whole analysis to the original images.

Immunofluorescence analysis. 50,000 cells were plated on 12 mm glass coverslips in a 24 well dish. The next day cells were fixed with 4% paraformaldehyde in 0.1M phosphate buffer (pH 7.2) for 20 minutes, washed and then blocked in 5% BSA + 0.1% saponin (Sigma) in PBS for 1 hour. This was followed by overnight staining with primary antibodies at 4 degrees, washing and 1 hour

staining with Alexa dye conjugated secondary antibodies (Thermo Fisher Scientific) at room temperature. Coverslips were then mounted on glass slides with Prolong Gold mounting media containing DAPI (Thermo Fisher Scientific).

Immunoblotting. After day 19 (human iPSC-derived macrophages) or day 40 (human iPSC-derived microglia) or day 7 (BMDM) of differentiation, cells were washed with ice-cold phosphate buffered saline and then lysed in radio-immunoprecipitation assay (RIPA) buffer (50mM Tris pH 7.4, 150 mM Nacl, 1% TX-100, 0.5% deoxycholate, 0.1% SDS) containing protease inhibitor and phosphatase inhibitor cocktails (Roche) and spun at 13,000 × g for 5 min. The supernatant was collected and incubated at 95°C for 3 min in SDS sample buffer before separation by SDS–PAGE on 4–15% gradient Mini-PROTEAN TGX precast polyacrylamide gels and transferred to nitrocellulose membranes (Bio-Rad, Hercules CA). Membranes were next blocked with 5% milk in TBS with 0.1% Tween 20 and incubated with primary antibodies and then HRP-coupled secondary antibodies in 5% milk or bovine serum albumin in TBS with 0.1% Tween 20. Chemiluminescence detection was performed on a Chemidoc MP imaging station (Bio-Rad), and FIJI/ImageJ was used to quantify band intensities[69].

RNA isolation and qRT PCR. Total RNA was extracted with the RNeasy kit (QIAGEN). cDNA was prepared from 1000 ng of RNA using the iScript cDNA synthesis kit (BIO-RAD). The total cDNA obtained was diluted 1:10 and 2 µl was used for qRT-PCR by using gene specific primer and SYBR green PCR mix (BIO-RAD) on BIO-RAD CFX96 real time PCR machine. Analysis was performed by calculating Δ and $2^{\Delta CT}$ values and mRNA expression levels for genes of interest was normalized to GAPDH and represented relative to control. Oligonucleotide primer sequences are provided in Table S1.

siRNA-mediated knockdown of TFE3. 100,000 cells were plated in a 100mm cell culture dish. The next day, siRNA transfections were performed with 20 µM siRNA, 40 µl RNAiMAX transfection reagent (Invitrogen), and 1,000 µl Opti-MEM (Invitrogen) that was added to 8 ml of

cell culture media. Experiments were performed 2 days post transfection. Tfe3 (5′-CAAACAGUACUUGUCUAC-3’ and 5’-AAGUGUGGUAGACAAGU-3) and control (5’-AUACGCGUAUUAUACGCGAUUAACGAC-3’ and 5’-CGUUAAUCGCGUAUAAUACGCGUAT -3’) siRNAs were purchased from Integrated DNA.

Statistical analysis. Statistical analysis was performed using Prism 8 software. Detailed statistical information (specific test performed, number of independent experiments, and p values) is presented in the respective figure legends.

Acknowledgements

We are grateful for microscopy resources provided by the Yale Program in Cellular Neuroscience, Neurodegeneration and Repair imaging facility. This research was supported by grants from the Parkinson’s Foundation, the Ludwig Foundation and Aligning Science Across Parkinson’s disease ASAP-000580 through the Michael J. Fox Foundation for Parkinson’s Research (MJFF). Agnes Roczniak-Ferguson (Yale), Amanda Bentley-DeSousa (Yale), Timothy Ryan (Cornell) and Pietro De Camilli (Yale) provided valuable feedback. We thank Mark Cookson (NIH) for sharing LRRK2 KO and G2019S knockin human iPSCs. We appreciate assistance from Maria Lara-Tejero (Yale) and Jorge Galan (Yale) with LRRK2 mutant mice. The authors do not have any conflicts to declare.

Author contributions

NY and SMF designed experiments. NY performed all experiments. NY and SMF analyzed data and prepared the manuscript.

Figure Legends

Figure 1. LRRK2 inhibits lysosomal protease activity in human iPSC-derived macrophages. **(A)** Airyscan live cell confocal micrographs showing tubular lysosome labeling in human iPSC-derived macrophages following labeling with DQ-BSA and Alexa488-BSA. Scale bar, 5 µm. **(B)** Confocal micrographs showing the DQ-BSA and Alexa488-BSA fluorescence in WT and LRRK2 KO macrophages treated with 0.1% DMSO (vehicle), 50 nM MLi-2 or 250 nM LRRK2-IN-1 for 3 hours. Scale bar, 10 µm. **(C)** The mean fluorescence intensity of DQ-BSA was normalized to BSA488 and plotted relative to DMSO control. The data was collected from 3 independent experiments with 60-80 cells per experiment. **(D)** Confocal micrographs showing the DQ-BSA and Alexa488-BSA fluorescence in WT and LRRK2 G2019S mutant macrophages. Scale bar, 10 µm. **(E)** Bar graph showing the quantification of DQ-BSA/BSA 488 fluorescence in WT and LRRK2 G2019S macrophages. The data was collected from 3 independent experiments with 60-80 cells per experiment. Error bars show mean ± SEM, one-way ANOVA, * $p<0.05$, ** $p< 0.01$, ***$p< 0.001$.

Figure 2: LRRK2 negatively regulates the levels of multiple lysosomal proteins in human iPSC-derived macrophages. (A) Immunoblot analysis of WT and LRRK2 KO macrophages treated with 0.1% DMSO (vehicle), 50 nM MLi-2 or 250 nM LRRK2-IN-1 for 6 hours. **(B-G)** Quantification of immunoblots in A. For samples where multiple bands reflect immature and mature cathepsin proteins, the quantification reflects the total of all bands. Data was collected from 3 independent experiments and plotted in relative to DMSO control cells. Error bars show mean ± SEM, one-way ANOVA, * $p<0.05$, ** $p< 0.01$, ***$p< 0.001$.

Figure 3: LRRK2 hyperactive Parkinson's mutation decreases levels of lysosomal proteins in human iPSC-derived macrophages. (A) Immunoblot analysis of WT and LRRK2 G2019S knockin macrophages treated with 0.1% DMSO (vehicle), 50 nM MLi-2 or 250 nM LRRK2-IN-1

for 6 hours. **(B-G)** Quantification of immunoblots in A. For samples where multiple bands reflect immature and mature cathepsin proteins, the quantification reflects the total of all bands. Data was collected from 3 independent experiments and plotted in relative to DMSO control cells. Error bars show mean ± SEM, one-way ANOVA, * p<0.05, ** p< 0.01, ***p< 0.001.

Figure 4: LRRK2 negative regulates the mRNA for multiple lysosome-related genes in human iPSC-derived macrophages. (A-D) qRT-PCR analysis of lysosomal transcripts (Cathepsin D, Cathepsin L, GBA and LAMP1) in WT and LRRK2 KO macrophages treated with 0.1% DMSO or 50 nM Mli-2 for 6 hours. Data was collected from 3 independent experiments, normalized to GAPDH and presented relative to DMSO control. **(D-G)** qRT-PCR analysis of lysosomal transcripts in WT and LRRK2 G2019S macrophages treated with 0.1% DMSO and 50nM Mli-2 for 6 hours. Data was collected from 3 independent experiments, normalized to GAPDH and presented relative to DMSO control. Error bars show mean ± SEM, one-way ANOVA, * p<0.05, ** p< 0.01, ***p< 0.001.

Figure 5: LRRK2 suppresses nuclear translocation of TFE3 in human iPSC-derived macrophages. (A) Immunofluorescence, confocal micrographs showing the sub cellular localization of TFE3 in WT and LRRK2 KO macrophages treated with 0.1% DMSO and 50nM Mli-2 for 6 hours. **(B)** Quantification of TFE3 nuclear localization under the indicated conditions where cells were scored for having nuclear>cytoplasmic TFE3 signal. Data was collected from 3 independent experiments, approximately 60-70 cells were analyzed per experiment. **(C)** Immunofluorescence, confocal micrographs showing the sub cellular localization of TFE3 in WT and LRRK2 G2019 mutant macrophages after treatment with 0.1% DMSO and 50nM Mli-2 for 6 hours. **(D)** Quantification of % cells with nuclear > cytoplasmic TFE3. Data was collected from 3 independent experiments, approximately 50-70 cells per experiment. **(E)** Immunoblots showing the impact of control and Tfe3 siRNAs on the levels of the indicated proteins in cells that were treated with 0.1% DMSO or 50nM Mli-2 for 6 hours. **(F-I)** Quantification of the abundance of the

indicated proteins from 3 independent experiments. Error bars show mean ± SEM, one-way ANOVA, * p<0.05, ** p< 0.01, ***p< 0.001).

Figure 6: LRRK2 negatively regulates the protein levels of TFE3 in human iPSC-derived macrophages. (A) Immunoblots showing the levels of TFE3 proteins in WT and LRRK2 macrophages cells treated with 0.1% DMSO, 50nM Mli-2 or 250nM LRRK2-in-1 for 6 hours. **(B)** Quantification of immunoblots in A. Data was collected from 3 independent experiments and plotted relative to DMSO-treated WT cells. **(C)** Immunoblots showing the levels of TFE3 in LRRK2 G2019S mutant macrophages treated with 0.1% DMSO or 50nM Mli-2 for 6 hours. **(D)** Quantification of immunoblots in E. Data was collected from 3 independent experiments and plotted relative to DMSO-treated WT cells. Error bars show mean ± SEM, one-way ANOVA, * p<0.05, ** p< 0.01, ***p< 0.001).

Figure 7: Regulation of human iPSC-derived microglial lysosomes by LRRK2 (A) Confocal micrographs showing DQ-BSA and Alexa488-BSA fluorescence in WT, LRRK2 KO and LRRK2 G2019S mutant macrophages treated with 0.1% DMSO or 50nM MLi2 for 3 hours. Scale bar, 10 µm. **(B)** Quantification of DQ-BSA/Alexa488-BSA fluorescence in WT, LRRK2 KO and LRRK2 G2019S mutant macrophages. The mean fluorescence intensity of DQ-BSA was normalized to BSA488 and plotted relative to the DMSO control. The data was collected from 3 independent experiments with 60-80 cells per experiment. **(C)** Immunoblot analysis of WT, LRRK2 KO and LRRK2 G2019S mutant microglia treated with 0.1% DMSO, 50nM MLi2 or 250 nM LRRK2-IN-1 for 6 hours. **(D-H)** Quantification of immunoblots for the indicated proteins from panel A. For the cathepsins, all bands (reflecting immature and mature proteins) were measured. Data was collected from 3 independent experiments, normalized to GAPDH abundance and plotted relative to DMSO-treated WT cells. **(I)** Immunoblots showing the levels of TFE3 protein in WT, LRRK2 KO and G2019S knockin microglia treated with 0.1% DMSO or 50 nM MLi2. **(J)** Quantification of immunoblots from panel I. Data was collected from 3 independent experiments and plotted in

relative to DMSO-treated WT cells. Error bars represent mean ± SEM; one-way ANOVA, * p<0.05, ** p< 0.01, ***p< 0.001.

Supplemental material

Fig. S1 shows the impact of LRRK2 perturbations on lysosomal protease activity in mouse BMDMs. Fig. S2 shows the impact of LRRK2 inhibition and KO on lysosome protein levels in mouse BMDMs. Fig. S3 shows the impact of LRRK2 inhibition and the G2019S mutation on lysosome protein levels in mouse BMDMs. Fig. S4 presents the regulation of TFE3 by LRRK2 in mouse BMDMs. Table 1 lists oligonucleotide primers used for qRT-PCR experiments.

References

1. Paisan-Ruiz C, Jain S, Evans EW, et al. Cloning of the gene containing mutations that cause PARK8-linked Parkinson's disease. *Neuron.* 2004;44(4):595-600.
2. Zimprich A, Biskup S, Leitner P, et al. Mutations in LRRK2 cause autosomal-dominant parkinsonism with pleomorphic pathology. *Neuron.* 2004;44(4):601-607.
3. Kluss JH, Mamais A, Cookson MR. LRRK2 links genetic and sporadic Parkinson's disease. *Biochem Soc Trans.* 2019;47(2):651-661.
4. Rocha EM, Keeney MT, Di Maio R, De Miranda BR, Greenamyre JT. LRRK2 and idiopathic Parkinson's disease. *Trends Neurosci.* 2022;45(3):224-236.
5. Wallings RL, Herrick MK, Tansey MG. LRRK2 at the Interface Between Peripheral and Central Immune Function in Parkinson's. *Front Neurosci.* 2020;14:443.
6. Zhang FR, Huang W, Chen SM, et al. Genomewide association study of leprosy. *N Engl J Med.* 2009;361(27):2609-2618.

7. Hui KY, Fernandez-Hernandez H, Hu J, et al. Functional variants in the LRRK2 gene confer shared effects on risk for Crohn's disease and Parkinson's disease. *Sci Transl Med.* 2018;10(423).

8. Jennings D, Huntwork-Rodriguez S, Henry AG, et al. Preclinical and clinical evaluation of the LRRK2 inhibitor DNL201 for Parkinson's disease. *Sci Transl Med.* 2022;14(648):eabj2658.

9. Taylor M, Alessi DR. Advances in elucidating the function of leucine-rich repeat protein kinase-2 in normal cells and Parkinson's disease. *Curr Opin Cell Biol.* 2020;63:102-113.

10. Kalogeropulou AF, Purlyte E, Tonelli F, et al. Impact of 100 LRRK2 variants linked to Parkinson's disease on kinase activity and microtubule binding. *Biochem J.* 2022;479(17):1759-1783.

11. Kuwahara T, Iwatsubo T. The Emerging Functions of LRRK2 and Rab GTPases in the Endolysosomal System. *Front Neurosci.* 2020;14:227.

12. Pfeffer SR. LRRK2 and Rab GTPases. *Biochem Soc Trans.* 2018;46(6):1707-1712.

13. Steger M, Tonelli F, Ito G, et al. Phosphoproteomics reveals that Parkinson's disease kinase LRRK2 regulates a subset of Rab GTPases. *Elife.* 2016;5.

14. Pfeffer SR. LRRK2 phosphorylation of Rab GTPases in Parkinson's disease. *FEBS Lett.* 2022.

15. Herbst S, Campbell P, Harvey J, et al. LRRK2 activation controls the repair of damaged endomembranes in macrophages. *EMBO J.* 2020;39(18):e104494.

16. Bonet-Ponce L, Beilina A, Williamson CD, et al. LRRK2 mediates tubulation and vesicle sorting from lysosomes. *Sci Adv.* 2020;6(46).

17. Eguchi T, Kuwahara T, Sakurai M, et al. LRRK2 and its substrate Rab GTPases are sequentially targeted onto stressed lysosomes and maintain their homeostasis. *Proc Natl Acad Sci U S A.* 2018;115(39):E9115-E9124.

18. Mamais A, Kluss JH, Bonet-Ponce L, et al. Mutations in LRRK2 linked to Parkinson disease sequester Rab8a to damaged lysosomes and regulate transferrin-mediated iron uptake in microglia. *PLoS Biol.* 2021;19(12):e3001480.

19. Pellegrini L, Hauser DN, Li Y, et al. Proteomic analysis reveals co-ordinated alterations in protein synthesis and degradation pathways in LRRK2 knockout mice. *Hum Mol Genet.* 2018;27(18):3257-3271.

20. Kluss JH, Mazza MC, Li Y, et al. Preclinical modeling of chronic inhibition of the Parkinson's disease associated kinase LRRK2 reveals altered function of the endolysosomal system in vivo. *Mol Neurodegener.* 2021;16(1):17.

21. Herzig MC, Kolly C, Persohn E, et al. LRRK2 protein levels are determined by kinase function and are crucial for kidney and lung homeostasis in mice. *Hum Mol Genet.* 2011;20(21):4209-4223.

22. Fuji RN, Flagella M, Baca M, et al. Effect of selective LRRK2 kinase inhibition on nonhuman primate lung. *Sci Transl Med.* 2015;7(273):273ra215.

23. Henry AG, Aghamohammadzadeh S, Samaroo H, et al. Pathogenic LRRK2 mutations, through increased kinase activity, produce enlarged lysosomes with reduced degradative capacity and increase ATP13A2 expression. *Hum Mol Genet.* 2015;24(21):6013-6028.

24. Ysselstein D, Nguyen M, Young TJ, et al. LRRK2 kinase activity regulates lysosomal glucocerebrosidase in neurons derived from Parkinson's disease patients. *Nat Commun.* 2019;10(1):5570.

25. Sanyal A, DeAndrade MP, Novis HS, et al. Lysosome and Inflammatory Defects in GBA1-Mutant Astrocytes Are Normalized by LRRK2 Inhibition. *Mov Disord.* 2020;35(5):760-773.

26. Sanyal A, Novis HS, Gasser E, Lin S, LaVoie MJ. LRRK2 Kinase Inhibition Rescues Deficits in Lysosome Function Due to Heterozygous GBA1 Expression in Human iPSC-Derived Neurons. *Front Neurosci.* 2020;14:442.

27. Kedariti M, Frattini E, Baden P, et al. LRRK2 kinase activity regulates GCase level and enzymatic activity differently depending on cell type in Parkinson's disease. *NPJ Parkinsons Dis.* 2022;8(1):92.

28. Klein AD, Mazzulli JR. Is Parkinson's disease a lysosomal disorder? *Brain.* 2018;141(8):2255-2262.

29. Ye H, Robak LA, Yu M, Cykowski M, Shulman JM. Genetics and Pathogenesis of Parkinson's Syndrome. *Annu Rev Pathol.* 2022.

30. Pan PY, Li X, Wang J, et al. Parkinson's Disease-Associated LRRK2 Hyperactive Kinase Mutant Disrupts Synaptic Vesicle Trafficking in Ventral Midbrain Neurons. *J Neurosci.* 2017;37(47):11366-11376.

31. Soukup SF, Kuenen S, Vanhauwaert R, et al. A LRRK2-Dependent EndophilinA Phosphoswitch Is Critical for Macroautophagy at Presynaptic Terminals. *Neuron.* 2016;92(4):829-844.

32. Brzozowski CF, Hijaz BA, Singh V, et al. Inhibition of LRRK2 kinase activity promotes anterograde axonal transport and presynaptic targeting of alpha-synuclein. *Acta Neuropathol Commun.* 2021;9(1):180.

33. Chen C, Soto G, Dumrongprechachan V, et al. Pathway-specific dysregulation of striatal excitatory synapses by LRRK2 mutations. *Elife.* 2020;9.

34. Hakimi M, Selvanantham T, Swinton E, et al. Parkinson's disease-linked LRRK2 is expressed in circulating and tissue immune cells and upregulated following recognition of microbial structures. *J Neural Transm (Vienna).* 2011;118(5):795-808.

35. Lee H, James WS, Cowley SA. LRRK2 in peripheral and central nervous system innate immunity: its link to Parkinson's disease. *Biochem Soc Trans.* 2017;45(1):131-139.

36. Moehle MS, Webber PJ, Tse T, et al. LRRK2 inhibition attenuates microglial inflammatory responses. *J Neurosci.* 2012;32(5):1602-1611.

37. Langston RG, Beilina A, Reed X, et al. Association of a common genetic variant with Parkinson's disease is mediated by microglia. *Sci Transl Med.* 2022;14(655):eabp8869.

38. Liu Z, Xu E, Zhao HT, Cole T, West AB. LRRK2 and Rab10 coordinate macropinocytosis to mediate immunological responses in phagocytes. *EMBO J.* 2020;39(20):e104862.

39. Lee H, Flynn R, Sharma I, et al. LRRK2 Is Recruited to Phagosomes and Co-recruits RAB8 and RAB10 in Human Pluripotent Stem Cell-Derived Macrophages. *Stem Cell Reports.* 2020;14(5):940-955.

40. Kuwahara T, Funakawa K, Komori T, et al. Roles of lysosomotropic agents on LRRK2 activation and Rab10 phosphorylation. *Neurobiol Dis.* 2020;145:105081.

41. Moehle MS, Daher JP, Hull TD, et al. The G2019S LRRK2 mutation increases myeloid cell chemotactic responses and enhances LRRK2 binding to actin-regulatory proteins. *Hum Mol Genet.* 2015;24(15):4250-4267.

42. Puertollano R, Ferguson SM, Brugarolas J, Ballabio A. The complex relationship between TFEB transcription factor phosphorylation and subcellular localization. *EMBO J.* 2018;37(11).

43. Palmieri M, Impey S, Kang H, et al. Characterization of the CLEAR network reveals an integrated control of cellular clearance pathways. *Hum Mol Genet.* 2011;20(19):3852-3866.

44. Pastore N, Brady OA, Diab HI, et al. TFEB and TFE3 cooperate in the regulation of the innate immune response in activated macrophages. *Autophagy.* 2016;12(8):1240-1258.

45. Shi J, Xue C, Liu W, Zhang H. Differentiation of Human-Induced Pluripotent Stem Cells to Macrophages for Disease Modeling and Functional Genomics. *Curr Protoc Stem Cell Biol.* 2019;48(1):e74.

46. Marwaha R, Sharma M. DQ-Red BSA Trafficking Assay in Cultured Cells to Assess Cargo Delivery to Lysosomes. *Bio Protoc.* 2017;7(19).

47. Sidransky E, Nalls MA, Aasly JO, et al. Multicenter analysis of glucocerebrosidase mutations in Parkinson's disease. *N Engl J Med.* 2009;361(17):1651-1661.

48. Sardiello M, Palmieri M, di Ronza A, et al. A gene network regulating lysosomal biogenesis and function. *Science.* 2009;325(5939):473-477.

49. Ferguson SM. Beyond indigestion: emerging roles for lysosome-based signaling in human disease. *Curr Opin Cell Biol.* 2015;35:59-68.

50. Martina JA, Diab HI, Lishu L, et al. The nutrient-responsive transcription factor TFE3 promotes autophagy, lysosomal biogenesis, and clearance of cellular debris. *Sci Signal.* 2014;7(309):ra9.

51. Roczniak-Ferguson A, Petit CS, Froehlich F, et al. The transcription factor TFEB links mTORC1 signaling to transcriptional control of lysosome homeostasis. *Sci Signal.* 2012;5(228):ra42.

52. Settembre C, Zoncu R, Medina DL, et al. A lysosome-to-nucleus signalling mechanism senses and regulates the lysosome via mTOR and TFEB. *EMBO J.* 2012;31(5):1095-1108.

53. Zhang Y, Chen K, Sloan SA, et al. An RNA-sequencing transcriptome and splicing database of glia, neurons, and vascular cells of the cerebral cortex. *J Neurosci.* 2014;34(36):11929-11947.

54. McQuade A, Coburn M, Tu CH, Hasselmann J, Davtyan H, Blurton-Jones M. Development and validation of a simplified method to generate human microglia from pluripotent stem cells. *Mol Neurodegener.* 2018;13(1):67.

55. Schmidt FI, Ploegh HL. Editorial: Crystal death: it's not always the inflammasome. *J Leukoc Biol.* 2017;102(1):1-4.

56. Alcalay RN, Hsieh F, Tengstrand E, et al. Higher Urine bis(Monoacylglycerol)Phosphate Levels in LRRK2 G2019S Mutation Carriers: Implications for Therapeutic Development. *Mov Disord.* 2020;35(1):134-141.

57. Xu Y, Du S, Marsh JA, et al. TFEB regulates lysosomal exocytosis of tau and its loss of function exacerbates tau pathology and spreading. *Mol Psychiatry.* 2021;26(10):5925-5939.

58. Martini-Stoica H, Xu Y, Ballabio A, Zheng H. The Autophagy-Lysosomal Pathway in Neurodegeneration: A TFEB Perspective. *Trends Neurosci.* 2016;39(4):221-234.

59. Contreras PS, Tapia PJ, Gonzalez-Hodar L, et al. c-Abl Inhibition Activates TFEB and Promotes Cellular Clearance in a Lysosomal Disorder. *iScience.* 2020;23(11):101691.

60. Napolitano G, Ballabio A. TFEB at a glance. *J Cell Sci.* 2016;129(13):2475-2481.

61. Baptista MAS, Merchant K, Barrett T, et al. LRRK2 inhibitors induce reversible changes in nonhuman primate lungs without measurable pulmonary deficits. *Sci Transl Med.* 2020;12(540).

62. Martina JA, Chen Y, Gucek M, Puertollano R. MTORC1 functions as a transcriptional regulator of autophagy by preventing nuclear transport of TFEB. *Autophagy.* 2012;8(6):903-914.

63. Wang X, Wu Y, Cai S, Ge J, Shao L, De Camilli P. Membrane remodeling properties of the Parkinson's disease protein LRRK2. *bioRxiv.* 2022.

64. Malek M, Wawrzyniak AM, Ebner M, Puchkov D, Haucke V. Inositol triphosphate-triggered calcium release from the endoplasmic reticulum induces lysosome biogenesis via TFEB/TFE3. *J Biol Chem.* 2022;298(3):101740.

65. Martina JA, Diab HI, Brady OA, Puertollano R. TFEB and TFE3 are novel components of the integrated stress response. *EMBO J.* 2016;35(5):479-495.

66. Medina DL, Di Paola S, Peluso I, et al. Lysosomal calcium signalling regulates autophagy through calcineurin and TFEB. *Nat Cell Biol.* 2015;17(3):288-299.

67. Beylina A, Langston RG, Rosen D, Reed X, Cookson MR. Generation of fourteen isogenic cell lines for Parkinson's disease-associated leucine-rich repeat kinase (LRRK2). *Stem Cell Res.* 2021;53:102354.

68. Yue M, Hinkle KM, Davies P, et al. Progressive dopaminergic alterations and mitochondrial abnormalities in LRRK2 G2019S knock-in mice. *Neurobiol Dis.* 2015;78:172-195.

69. Schindelin J, Arganda-Carreras I, Frise E, et al. Fiji: an open-source platform for biological-image analysis. *Nat Methods.* 2012;9(7):676-682.

Figure 1

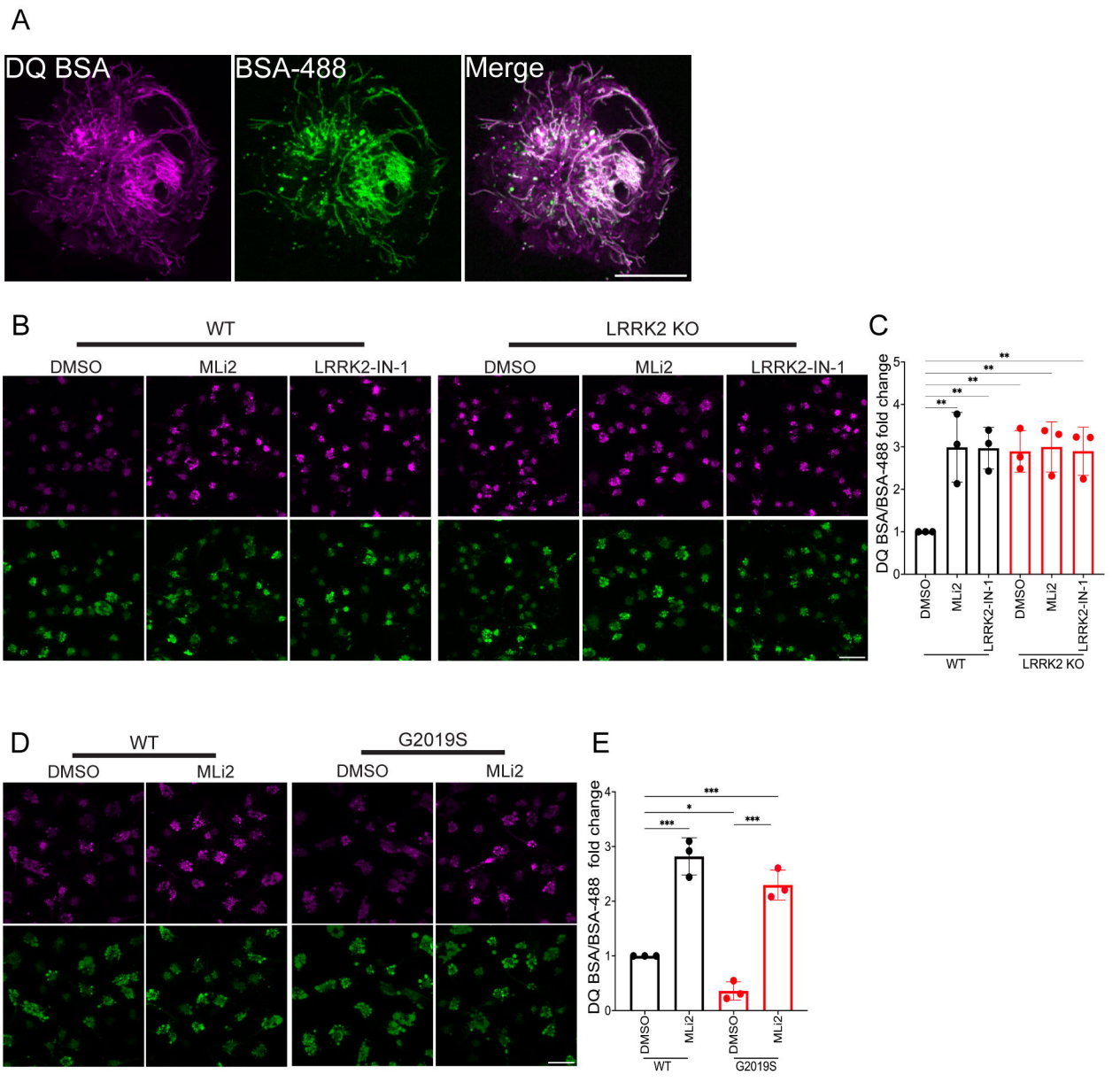
A
DQ BSA
BSA-488
Merge
B
WT
LRRK2 KO
DMSO
MLi2
LRRK2-IN-1
DQ BSA
BSA-488
C
DQ BSA/BSA-488 fold change
WT
LRRK2 KO
D
G2019S
E

Figure 2

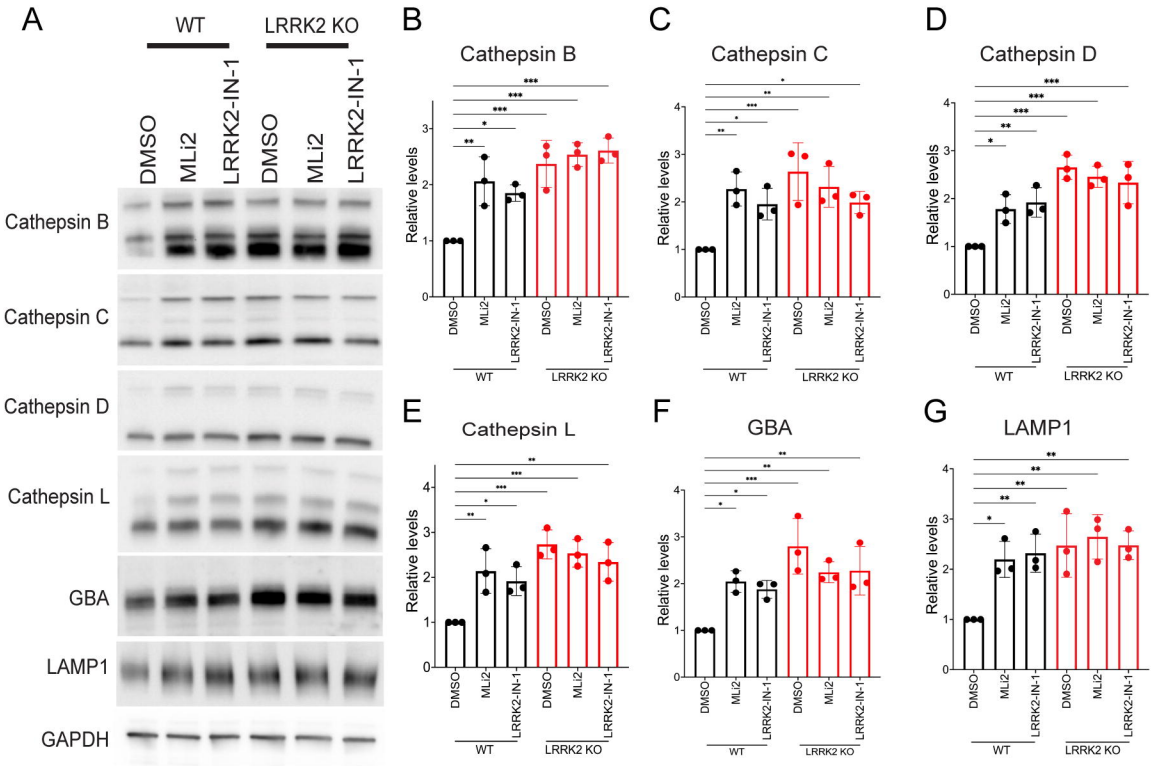
A
WT
LRRK2 KO
DMSO
MLi2
LRRK2-IN-1
DMSO
MLi2
LRRK2-IN-1
Cathepsin B
Cathepsin C
Cathepsin D
Cathepsin L
GBA
LAMP1
GAPDH
B
Cathepsin B
C
Cathepsin C
D
Cathepsin D
E
Cathepsin L
F
GBA
G
LAMP1
Relative levels
DMSO
MLi2
LRRK2-IN-1
WT
LRRK2 KO

Figure 3

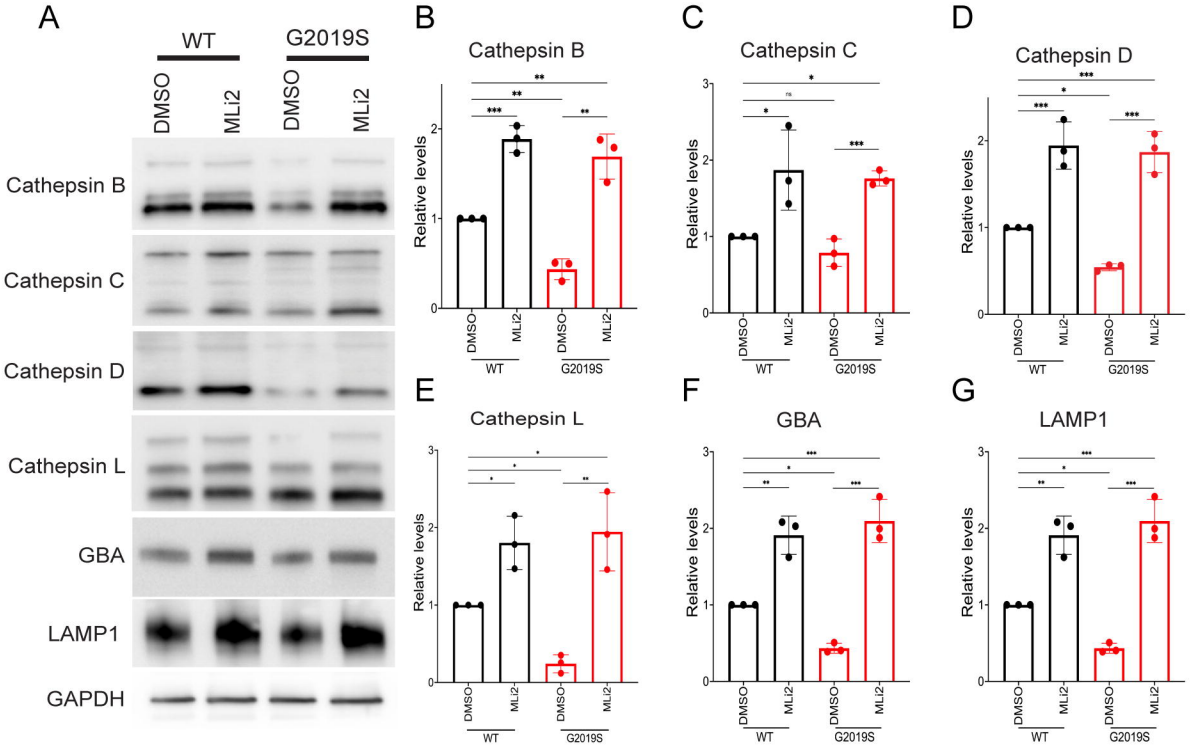
A
WT
G2019S
DMSO
MLi2
DMSO
MLi2
Cathepsin B
Cathepsin C
Cathepsin D
Cathepsin L
GBA
LAMP1
GAPDH
B
Cathepsin B
C
Cathepsin C
D
Cathepsin D
E
Cathepsin L
F
GBA
G
LAMP1
Relative levels
DMSO
MLi2
WT
G2019S

Figure 4

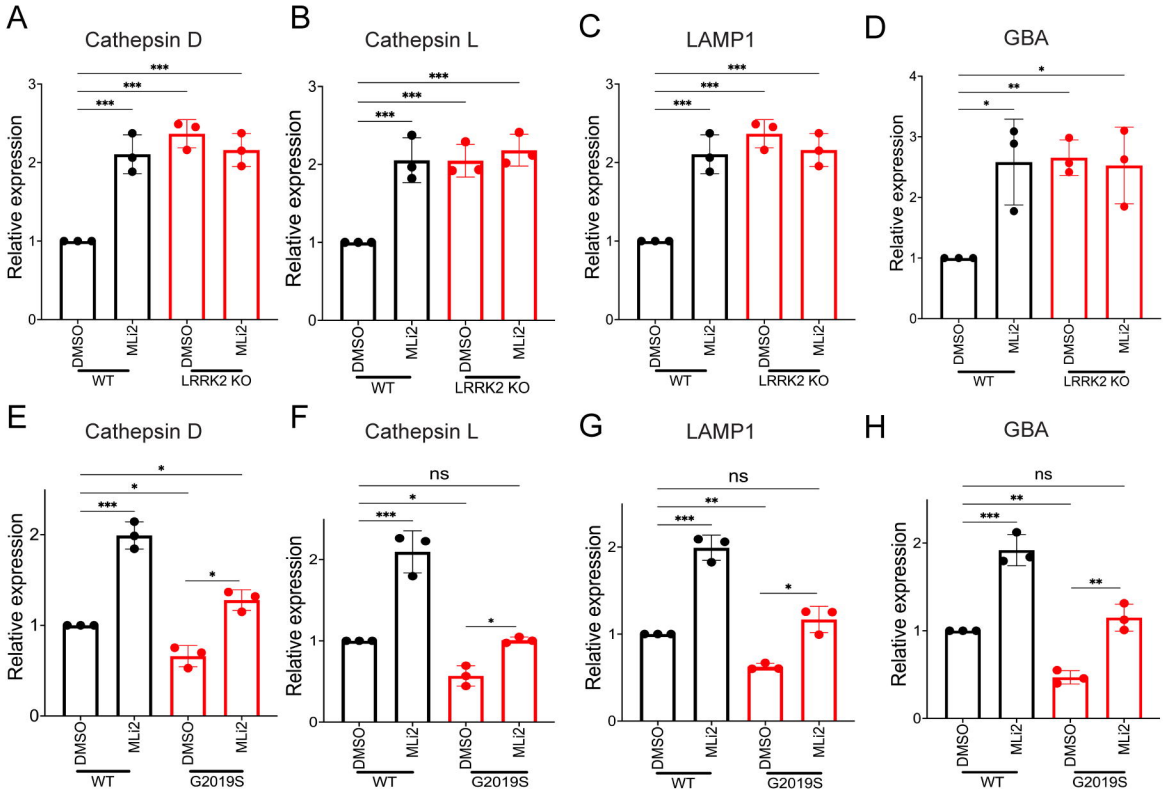
A
Cathepsin D
B
Cathepsin L
C
LAMP1
D
GBA
Relative expression
DMSO
MLi2
WT
LRRK2 KO
E
Cathepsin D
F
Cathepsin L
G
LAMP1
H
GBA
G2019S
ns

Figure 5

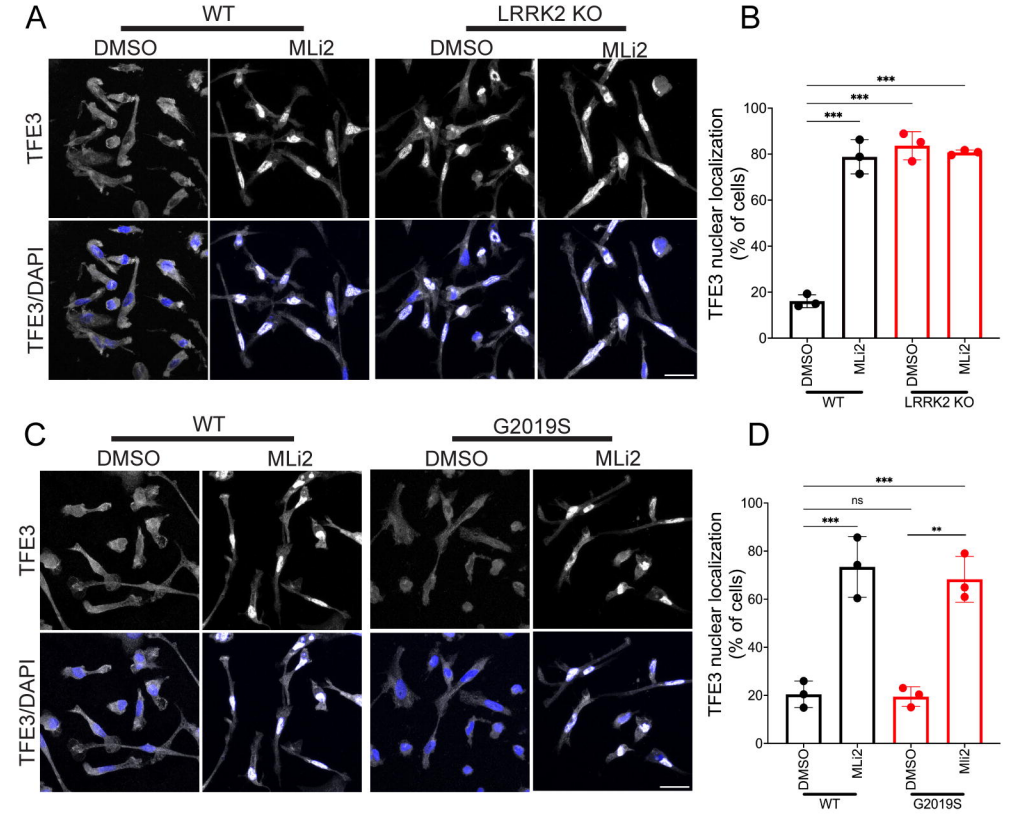
A
WT
LRRK2 KO
DMSO
MLi2
DMSO
MLi2
TFE3
TFE3/DAPI
B
TFE3 nuclear localization (% of cells)
***
***
***
DMSO
MLi2
DMSO
MLi2
WT
LRRK2 KO
C
WT
G2019S
DMSO
MLi2
DMSO
MLi2
TFE3
TFE3/DAPI
D
TFE3 nuclear localization (% of cells)
***
ns
***
**
DMSO
MLi2
DMSO
MLi2
WT
G2019S

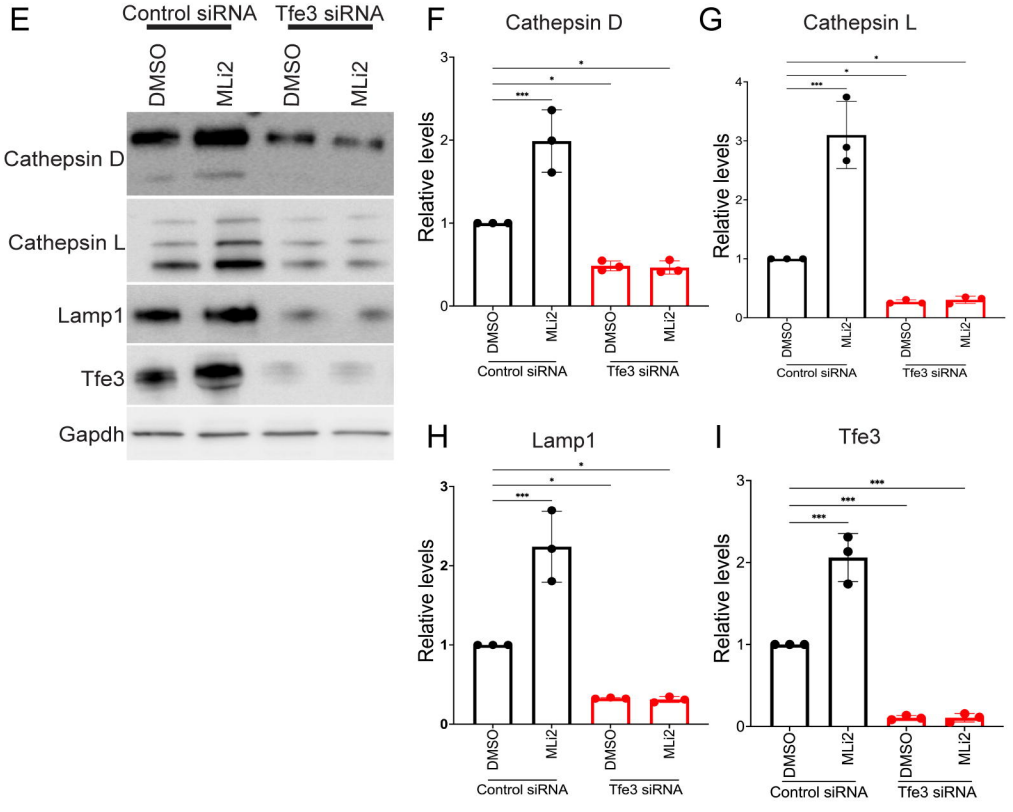
E
Control siRNA
Tfe3 siRNA
DMSO
MLi2
DMSO
MLi2
Cathepsin D
Cathepsin L
Lamp1
Tfe3
Gapdh
F
Cathepsin D
Relative levels
DMSO
MLi2
DMSO
MLi2
Control siRNA
Tfe3 siRNA
G
Cathepsin L
Relative levels
DMSO
MLi2
DMSO
MLi2
Control siRNA
Tfe3 siRNA
H
Lamp1
Relative levels
DMSO
MLi2
DMSO
MLi2
Control siRNA
Tfe3 siRNA
I
Tfe3
Relative levels
DMSO
MLi2
DMSO
MLi2
Control siRNA
Tfe3 siRNA

Figure 6

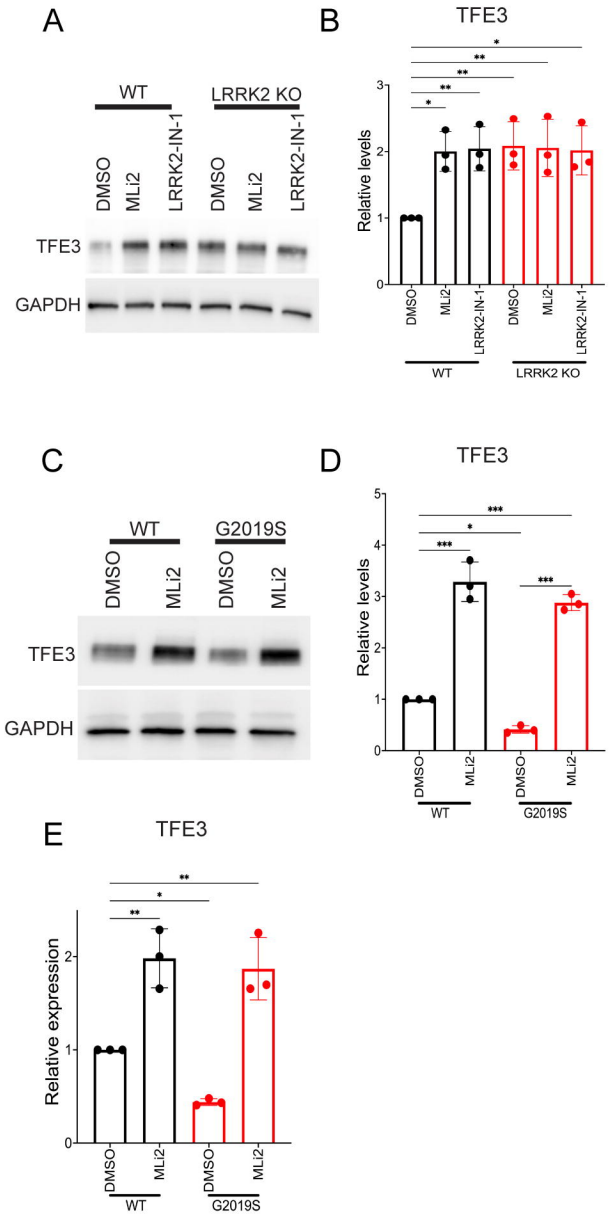
A
WT
LRRK2 KO
DMSO
MLi2
LRRK2-IN-1
DMSO
MLi2
LRRK2-IN-1
TFE3
GAPDH
B
TFE3
Relative levels
0
1
2
3
*
**
**
**
*
DMSO
MLi2
LRRK2-IN-1
DMSO
MLi2
LRRK2-IN-1
WT
LRRK2 KO
C
WT
G2019S
DMSO
MLi2
DMSO
MLi2
TFE3
GAPDH
D
TFE3
Relative levels
0
1
2
3
4
5
***
*
***
***
DMSO
MLi2
DMSO
MLi2
WT
G2019S
E
TFE3
Relative expression
0
1
2
**
*
**
DMSO
MLi2
DMSO
MLi2
WT
G2019S

Figure 7

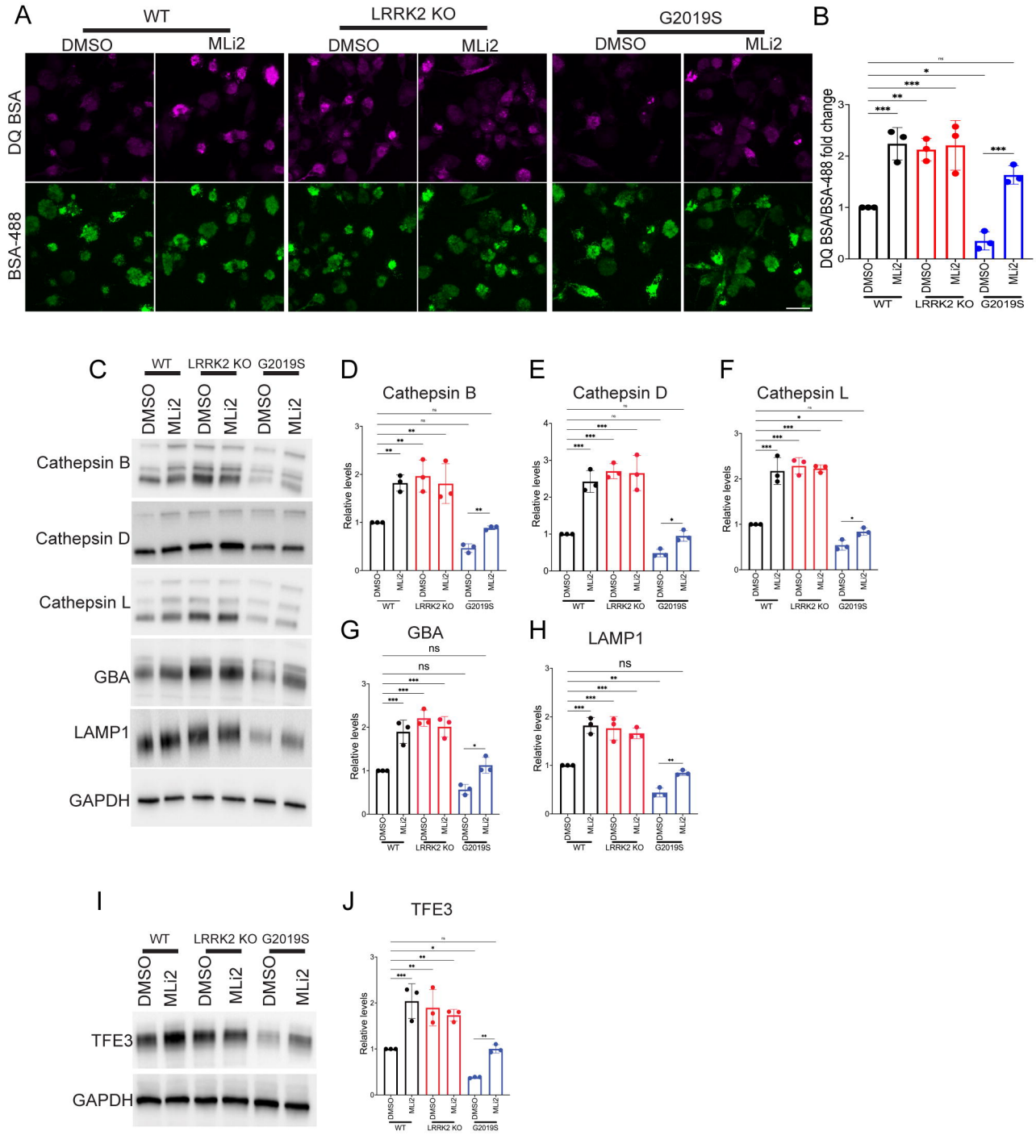
A
WT
LRRK2 KO
G2019S
DMSO
MLi2
DQ BSA
BSA-488
B
DQ BSA/BSA-488 fold change
C
Cathepsin B
Cathepsin D
Cathepsin L
GBA
LAMP1
GAPDH
D
Cathepsin B
E
Cathepsin D
F
Cathepsin L
G
GBA
H
LAMP1
I
TFE3
GAPDH
J
TFE3
Relative levels